You can view the Version of Record for this article at: https://doi.org/10.1088/1361-6463/ace456

A New Numerical Approach for Efficient Modeling of Positive Corona Discharge and its Associated Electric Wind

K. Yanallah[1*], A. Chelih[2], M.R. Bouazza[1], F. Pontiga[3*], M. Bouadi[1], P. A. Vázquez[4], and Z. Bendaoudi[5,6]

[1]Dpt. of Physics, Faculty of Sciences of Matter, LGEP Laboratory, University of Tiaret, Algeria

[2]Dpt. of Electrical Engineering, Faculty of Applied Sciences, LGEP Laboratory, University of Tiaret, Algeria

[3]Departamento de Física Aplicada II, Universidad de Sevilla, Spain

[4]Departamento de Física Aplicada III, Universidad de Sevilla, Spain

[5]Dpt. of Automatics and Electrical Engineering, Faculty of Science and Technology, University of Relizane, Algeria

[6]APELEC Laboratory, Djillali Liabes University of Sidi Bel-Abbes, Algeria

Keywords: *Corona discharge, numerical modeling, electric wind*

Abstract

Research on corona wind generation has been increasing in recent years because of its potential technological applications, particularly those related to improving heat transfer in small-scale devices. Since numerical simulations play a key role in the design of these applications, computationally efficient modeling of corona discharge is imperative. This work presents a new approach that allows rapid computation of the electrohydrodynamic force density responsible for the generation of electric wind. Arbitrary electrode configurations can easily be dealt with in the model, since only the Laplacian electric field lines have to be determined numerically. Then, using approximated analytical approximations of the electric field intensity along the field lines, the spatial distribution of the current density and the space charge density can be easily determined. The model has been satisfactorily tested against experimental measurements of the current-voltage characteristic and the current density distribution on the cathode. Furthermore, the electric wind computed from the electrohydrodynamic force agrees quite satisfactorily with measurements carried out in different electrode configurations. Finally, the model has been applied to a new electrode configuration that has greater potential for heat transfer applications.

1. Introduction

As is well known, corona discharge is a strongly non-equilibrium weakly ionized plasma that is generated between two electrodes with highly asymmetric geometry. Generally, one electrode is a small-diameter wire, needle, or sharp blade, while the other is usually a plane or a large-diameter cylinder. The active corona region only exists in the immediate vicinity of the electrode with singular geometry, where reinforcement of the electric field causes electrical breakdown and ionization.

* Authors to whom any correspondence should be addressed.

Corona discharge processes have been widely used in many industrial and commercial applications for a long time [1]. For example, corona discharge is used as an ion source in electrostatic precipitators and xerographic machines. In addition, corona-induced plasma reactors have found applications in flue gas treatment, for the removal of NO_x, SO_x, volatile organic compounds, and other hazardous emissions. Another effect associated with corona discharge is the direct conversion of electrical energy into kinetic energy (electrohydrodynamic effect), a phenomenon often referred to as the ionic wind or the electric wind. The electrohydrodynamic (EHD) motion of the gas arises as a result of momentum transfer through collisions between the ions, which drift under the electric field, and the neutral molecules of the gas. Although the phenomenon of corona-induced EHD gas motion has long been known, it remains a complex problem, and research on this topic has multiplied in recent decades due to its many interesting applications [2, 3], such as fluid pumping [4, 5], enhancement of heat transfer [6], evaporation and drying [7, 8], electrohydrodynamic thrusters [9, 10], or airflow control [11].

The first step in the modeling of the ionic wind is to calculate the electric field, the space charge density, and the EHD force density, which usually requires solving a system of coupled electrical equations composed of the Gauss equation and the continuity equations of the charged particles. Once the EHD force density is obtained, the next step is to solve the Navier-Stokes equations, to determine the spatial distribution of the gas velocity generated by the EHD force. The system of electrical equations and the Navier-Stokes equations can be solved separately because the electric drift velocity of ions ($\sim 10^2$ m/s) is, typically, two orders of magnitude higher than the electric wind velocity (~ 1 m/s). However, in certain applications of corona discharge, such as airflow control around airfoils [11], or corona discharge in air with high wind speeds [12], the background velocity of the gas can affect electric drift of ions. In such cases, the electrical equations and the Navier-Stokes equations cannot be decoupled.

The solution of electrical equations has been approached with a wide variety of numerical techniques. For instance, early studies by Atten [13] and McDonald et al. [14] used the finite difference method (FDM) to iteratively solve the Gauss equation coupled with the continuity equation. Davies and Hoburg [15] proposed an alternative technique, employing the finite element method (FEM) combined with the method of characteristics (MOC). However, in these studies, the charge density on the wire is taken as a boundary condition and, since it is unknown, different strategies must be followed to determine its value. According to the method proposed by Kaptsov [16], the narrow ionization region around the coronating electrode can be dealt as an effective boundary condition for the electric field. This approach, often referred to as Kaptsov's assumption, states that electric field on the corona wire remains constant at the threshold value for corona onset. This approximation has been used by Zhao and Adamiak [17, 18] to evaluate the charge density on the corona electrode surface in the simulation of corona discharge in pin-plate and pin-grid configurations. They developed a hybrid numerical algorithm based on the boundary element method, the finite element method, and the method of characteristics. Other numerical techniques employed by researchers include combining FEM and a donor cell method [19], using pseudotransient

relaxation and finite volume discretization (FVM) [20], or implementing a particle-in-cell (PIC) method to simulate transient corona [21].

Although all these numerical approaches have certainly helped improve our understanding of corona discharge, their implementation can be complex and computationally expensive. Furthermore, after solving the electrical equations, the Navier-Stokes equations must be integrated, which is normally done using computational fluid dynamics (CFD) simulations based on FEM or FVM [17, 18]. Therefore, to speed up the computation time, asymptotic and semi-analytical models of the stationary corona discharge have been developed in the past. For example, Seimandi et al. [22] have proposed an asymptotic model for wire-to-wire corona discharges that divides the discharge space into two narrow ionization regions around the electrodes and one larger region between them. Inside each region, they established a simplified quasi-analytical solution for the electric field and the space charge. This solution is then used to estimate the velocity of the ionic wind. In previous studies, the authors have also obtained semi-analytical solutions of the corona discharge [23, 24, 25], which provided simple relations for the spatial distributions of electrons, ions, electric field, and the EHD force density. Using this information, the ionic wind has been successfully simulated [26, 27, 28]. However, these semi-analytical solutions are only applicable to simple electrode configurations, such as wire-to-cylinder, wire-to-plate, and point-to-plate.

In the present study, we introduce a new approach that allows us to handle complex electrode configurations. Only the Laplacian electric field needs to be numerically integrated in order to determine the electric field lines. Then, using the semi-analytical formulations previously developed, satisfactory approximations of the electric field and the space charge density are obtained, which helps to determine the EHD force density. Therefore, the proposed method is easy to implement and computationally very efficient, as it does not require iterating on an unstructured mesh to solve the electrical equations, which is usually required in FEM or FVM. Furthermore, it avoids the convergence problems that may arise when solving the Gauss equation coupled to the continuity equations of the charged species. By optimizing the modeling process, we aim to be able to perform more accurate and realistic simulations of the corona discharge and the electrical wind over a wide variety of electrode configurations.

2. Governing equations

2.1 Electrical modeling

The corona discharge for positive polarity can be successfully simulated by solving the continuity equations for the charged particles coupled with the Gauss law. The continuity equations quantitatively describe the transport and the gain/loss balance of the charged particles due to the chemical reactions induced by the electrical discharge. Generally, in the case of a positive corona, only two generic types of charged particles (electrons and positive ions) need to be considered for the physical modeling [25]. In the stationary regime, the governing equations can be expressed as follows:

$$-\nabla \cdot \mathbf{J}_e = \alpha \left| \mathbf{J}_e \right|, \tag{1}$$

$$\nabla \cdot \mathbf{J}_p = \alpha \left| \mathbf{J}_e \right|, \tag{2}$$

$$\nabla \cdot \mathbf{E} = \frac{e_0}{\varepsilon_0}\left(N_p - N_e \right), \tag{3}$$

$$\mathbf{J}_e = \mu_e N_e \mathbf{E}, \text{ and } \mathbf{J}_p = \mu_p N_p \mathbf{E}, \tag{4}$$

where subscripts e and p correspond to electrons and positive ions, respectively; N_e and N_p are the number densities of the particles, with mobilities μ_e and μ_p, respectively; ε_0 is the gas permittivity; e_0 is the positive elementary charge; and α is the ionization coefficient, which depends on the intensity of the electric field $\mathbf{E}$ [29]. The contributions of convection and diffusion to $\mathbf{J}_e$ and $\mathbf{J}_p$ have been neglected, since the electron and ion drift velocities are much higher than electric wind velocity and the diffusion velocities [30].

Since both the drift of electrons and ions are parallel to the electric field, the system of partial differential equations (1)-(3) can be transformed into a system of ordinary differential equations using the electric field lines as coordinate lines. Thus, applying the divergence theorem to a flux tube of electric field lines (see figure 1), the governing equations along any field line can be written as

$$-\frac{1}{\Delta S}\frac{d}{dl}\left[\Delta S J_e\right] = \alpha J_e, \tag{5}$$

$$\frac{1}{\Delta S}\frac{d}{dl}\left[\Delta S J_p\right] = \alpha J_e, \tag{6}$$

$$\frac{1}{\Delta S}\frac{d}{dl}\left[\Delta S E\right] = \frac{e_0}{\varepsilon_0}\left(N_p - N_e \right), \tag{7}$$

where J_e, J_p, and E are the magnitudes of their corresponding vectors, dl is an infinitesimal displacement along the electric field line, and ΔS is an element of surface perpendicular to the field line, which is a function of l (the arc length along the field line). If the physical problem has continuous translational symmetry (2D problem), ΔS reduces to an elementary line segment perpendicular to the field line. Subtraction of (5) and (6) shows that the product of the electric current density, $j = e_0(J_e + J_p)$, and ΔS is constant along the field line, that is, $j\Delta S =$ const.

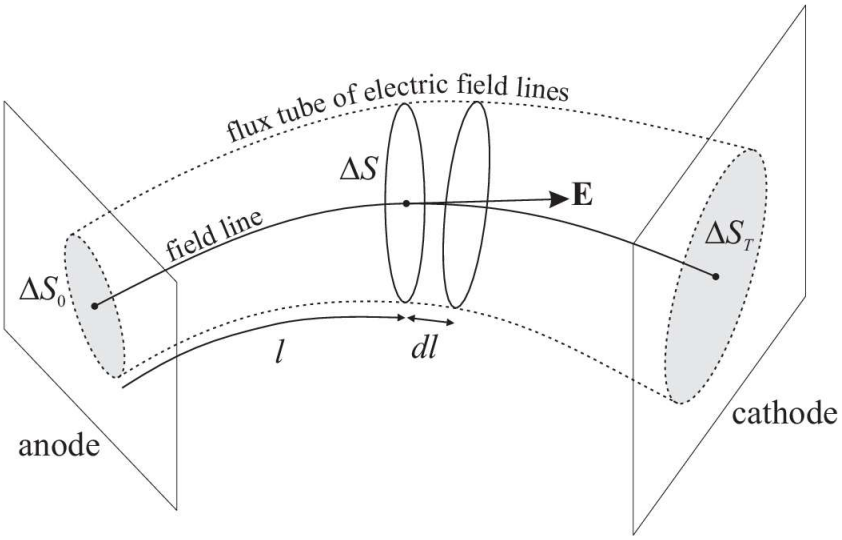

Figure 1. Schematic illustration of a flux tube of electric field lines connecting the anode and the cathode.

In the positive corona, the space charge is mostly due to the positive ions. Therefore, as shown in previous works [25], the magnitude of the electric field along the field line can be obtained by direct integration of (7), which gives

$$E(l) = \frac{1}{\Delta S}\sqrt{(\Delta S_0 E_0)^2 + c_p \Delta S_T \int_0^l \Delta S \, dl}, \tag{8}$$

where subscripts 0 and T denote that the corresponding physical quantities are evaluated at the corona electrode and at the ground (the cathode), respectively, and $c_p = 2j_T/(\varepsilon_0 \mu_p)$, where j_T is the current density at the cathode.

The value of E_0 can be determined using Kaptsov's assumption, which states that the electric field on the corona electrode remains constant for a wide range of applied voltages. Therefore, Peek's law for the threshold field of corona discharge can be used to obtain E_0. Kaptsov's hypothesis is especially suitable for corona wires centered inside axisymmetric grounded electrodes, or corona wires away from grounded electrodes, since these configurations favor the charge density and electric field to be constant at any plane section of the corona wire [31]. However, refined simulations of corona discharge in hyperbolic point-plane configuration using direct ionization criteria show that Kaptsov's hypothesis, even if it may not be entirely accurate, does not introduce significant errors in predicting the total corona current [32]. Of course, some deviations can be expected with increasing voltage, as the effect of the space charge becomes more important. Kaptsov's hypothesis may not be applicable to corona discharge with high gas velocities, which can modify the space charge distribution [12].

For single curvature corona electrodes, which is the case for wires, the electric field on the corona electrode predicted by Peek's law is given as [33]

$$E_0 = 31 \text{ kV cm}^{-1} \, \delta \left(1 + \frac{0.308}{\sqrt{\delta r_0}} \right), \tag{9}$$

where r_0 is the radius of the wire in cm and $\delta = (p/p_0)/(T/T_0)$ is an environmental factor that depends on the ratios of the actual gas pressure to the atmospheric pressure (p_0 = 101325 Pa), and the actual gas temperature to the room temperature (T_0 = 298 K). For electrodes with double curvature (e.g., needles, spheres, etc.), Peek's equation can still be used provided that r_0 is replaced by an equivalent radius, which is defined as $R_{eq} = (R_1^{-1} + R_2^{-1})^{-1}$, where R_1 and R_2 are the principal curvature radii at the given point on the corona electrode [32, 33].

In complex geometries, the numerical integration of the set of partial differential equations (1)-(3) can often be time consuming. However, using (8) and adopting the Deutsch assumption of undistorted field lines [34], the solution of the problem can be reduced to integrating only the Laplace equation, followed by an iterative root-finding algorithm. This strategy, which is schematically presented in figure 2, consists of the following steps:

1. Numerically integrating Laplace's equation for the electric potential, ϕ, subjected to the appropriate boundary conditions:

$$\nabla^2 \phi = 0, \tag{10}$$

where the electric potential at the anode (the corona electrode) is fixed, $\phi = V$, and at the cathode it is zero, $\phi = 0$.

2. Calculating the electric field,

$$E = -\nabla \phi. \tag{11}$$

3. Computing the electric field lines and the value of ΔS along the field lines.

4. Assigning a trial value to the current density on the cathode, j_T.

5. Computing the magnitude of the electric field along the field lines using (8) and (9).

6. Evaluating the path integral of the electric field between the anode and the cathode along the field lines,

$$\phi_0 = -\int_0^L E\, dl, \tag{12}$$

where L is the total length of the electric field line.

7. Testing whether the difference between V and ϕ_0 meets the desired convergence criterion, ζ,

$$\left|\phi_0 - V\right| < \zeta \tag{13}$$

If it does not, the value of j_T must be decreased if $\phi_0 > V$, or, conversely, it must be increased if $\phi_0 < V$. Steps 5 to 7 are then repeated until the convergence criterion is finally satisfied.

When the convergence criterion is met, both the electric field magnitude inside the physical domain and the electric current density on the cathode are then known. Therefore, the current

density and the (positive) space charge density at any point in interelectrode space can be determined as

$$j = \frac{j_T \Delta S_T}{\Delta S}, \tag{14}$$

$$q_p = e_0 N_p = \frac{j_T \Delta S_T}{\mu_p E \Delta S}. \tag{15}$$

Therefore, if a more accurate solution is required, the process can be restarted by integrating Poisson's equation in place of Laplace's equation, using the computed space charge density.

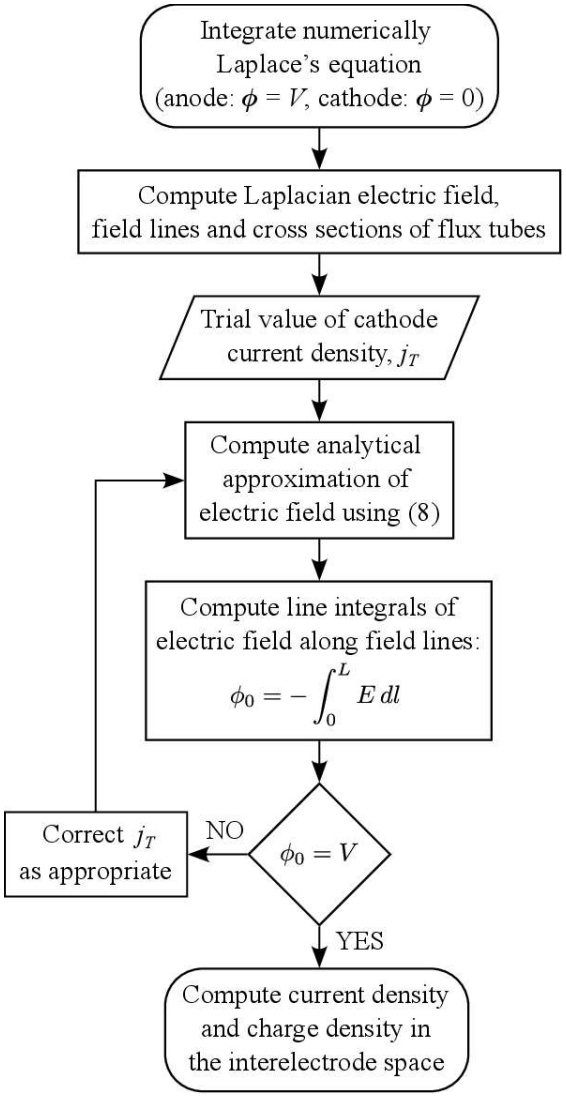

Figure 2. Flow chart of the calculation procedure.

2.2 Mechanical modeling

When positive corona discharge occurs, the ions generated by the corona discharge are accelerated and transfer part of their momentum to the neutral gas molecules through ion-molecule collisions. Consequently, an electrohydrodynamic gas flow appears with velocities

of up to several meters per second, which can be successfully described by means of the Navier–Stokes equations. Assuming that the air flow is incompressible and stationary, the Navier–Stokes equations can be written as follows,

$$\nabla \cdot \mathbf{v} = 0\,, \tag{16}$$

$$\rho(\mathbf{v} \cdot \nabla \mathbf{v}) = -\nabla p + \eta \nabla^2 \mathbf{v} + \mathbf{F}\,, \tag{17}$$

where $\mathbf{v}$ and p are, respectively, the fluid velocity and gas pressure, ρ is the air density, and η is its dynamic viscosity. The most important contribution to the EHD force is the Coulomb force, which can be obtained as [27]

$$F = \frac{1}{\mu_p} \frac{j_T \Delta S_T}{\Delta S}\,. \tag{18}$$

3. Results and discussion

In this section, the accuracy of the numerical modeling proposed in the previous section will be first tested by comparing their predictions with experimental measurements reported in the literature. The tests are aimed at twofold validation: (1) electrical, to demonstrate the ability of the numerical modeling to accurately predict the current-voltage characteristic of the corona discharge and the spatial distribution of the current intensity on the cathode, and (2) electrohydrodynamic, to demonstrate its capability to quantitatively describe the ionic wind generated by the corona discharge. After setting the validity of the numerical technique, the problem of EHD pumping between two parallel plates using positive corona discharge will be addressed.

3.1 Numerical validation

Electrical validation

The wire-duct electrode configuration (Fig. 3) is frequently used as a case study in the research of electrostatic precipitators. The corona wire, with radius r_0, is subjected to high voltage, while the plates, separated from the wire by a distance d, are connected to ground. Due to the symmetry of this configuration, the study of this problem can be made in 2D. Therefore, as explained in section 2.1, the elementary normal section of the flux tube of electric field lines, ΔS, becomes the line segment P_1P_2.

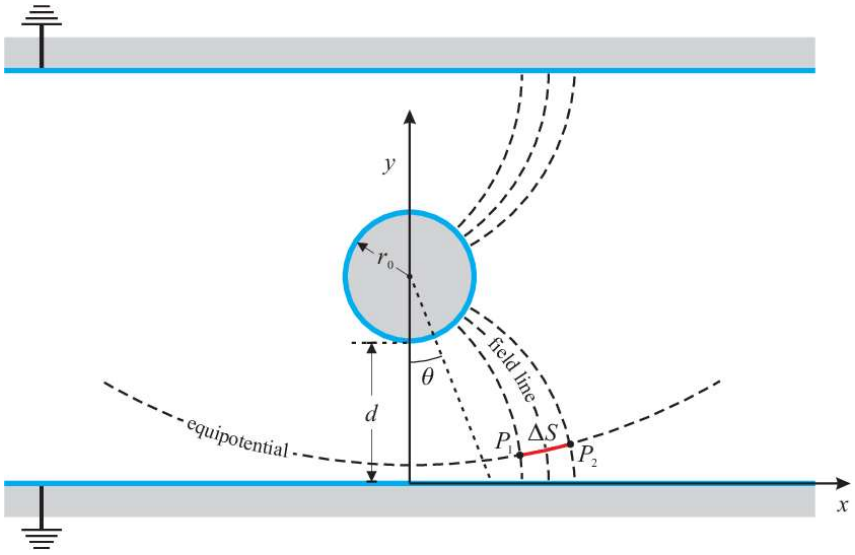

Figure 3. Schematic representation of a wire-duct electrostatic precipitator (not to scale).

Among other researchers, Yamamoto and Velkoff [35] have investigated experimentally and numerically different variations of this electrode configuration. In their experimental set-up, they use a corona discharge wire 19 cm in length with a radius r_0 = 0.1 mm and a wire-to-plate spacing d = 2.9 cm. The wire is subjected to a high positive electrical potential in the range 10 kV to 17.5 kV.

In figure 4, the experimental measurements of the current intensity reported in [35] for different applied voltages are compared with the numerical results obtained in the present study for the same geometrical parameters. Clearly, the agreement with the experimental measurements is quite satisfactory. The current-voltage characteristic follows the classical law $i = k\,V(V - V_0)$, where k is constant and V_0 is the corona inception voltage [34, 36].

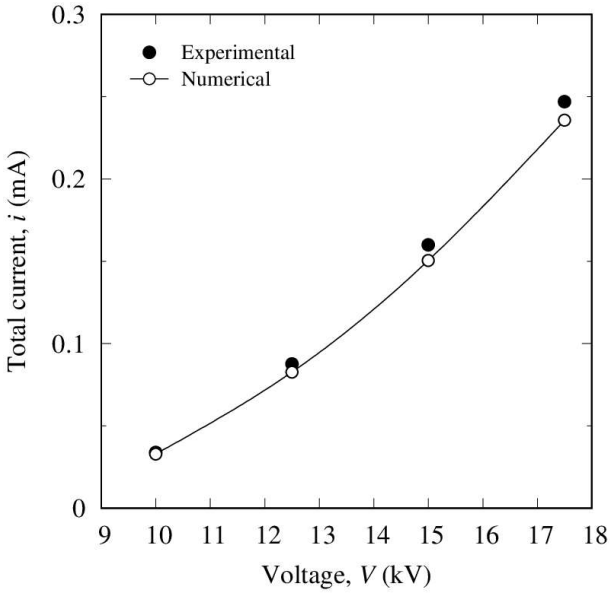

Figure 4. Current-voltage characteristic of a positive corona wire-duct electrostatic precipitator, for a wire radius r_0 = 0.1 mm and a wire-plate separation d = 2.9 cm. The experimental points (solid circles) correspond to the measurements of Yamamoto and Velkoff [35].

Yamamoto and Velkoff [35] were also able to measure the current density distribution on the cathode using an array of 1.6 mm diameter brass rods spaced 6.4 mm apart. The current density at any rod was read by a micro-ammeter connected to it, while the rest of the rods were grounded. These measurements are compared with the results of the present numerical modeling in figure 5. The current density is normalized with its maximum value, which is reached at $x = 0$ cm, beneath the wire. Again, the agreement between numerical simulation and experiment is quite satisfactory. The current distribution follows a $\cos^m \theta$ Warburg-type law, with $m \approx 4$.

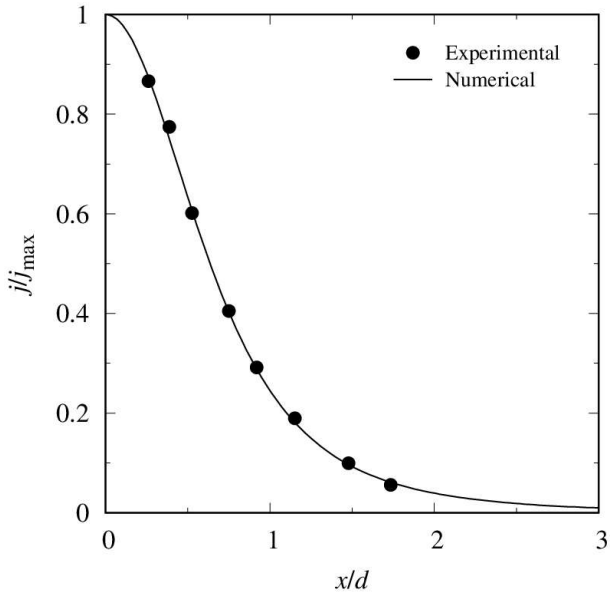

Figure 5. Normalized current density distribution on the cathode of a wire-duct electrostatic precipitator for an applied voltage of +15 kV (wire radius: $r_0 = 0.1$ mm, wire-plate separation: $d = 2.9$ cm). The experimental points (circles) correspond to the measurements of Yamamoto and Velkoff [35].

Electrohydrodynamic validation

To determine the gas velocity distribution generated by the corona discharge, the driving force of the gas motion (*i.e.*, the electrohydrodynamic force) must be first evaluated from the solution of the electrical equations, using (18). Then, the Navier-Stokes equations (16)-(17) must be integrated assuming the no-slip condition at all solid boundaries. Here, the open-source solver OpenFOAM [37], a CFD software based on the finite-volume method, will be used for that purpose. OpenFOAM is adequate for modeling both laminar and turbulent flows. When dealing with fluid flows confined in narrow channels, the fluid simulation will be performed assuming laminar flow, since Reynolds number will not exceed the critical value for the onset of turbulence. However, in other configurations, where the flow is expected to be turbulent, the RANS k-epsilon turbulence model will be chosen.

The electrohydrodynamic validation will be carried out by comparing the results of the numerical modeling with the experimental measurements of the gas velocity reported for two different electrode arrangements: parallel wire-plate and wire-duct. The first one has been experimentally investigated by Elagin et al. [38], who measured the gas velocity distribution using particle image velocimetry (PIV). Among other configurations, they used a corona wire

with radius r_0 = 50 μm and a wire-plate separation d = 15 mm. The electric potential applied to the wire was varied in the range 5–13.5 kV.

Figure 6 shows the spatial distribution of the magnitude of the EHD force calculated numerically for the same electrode configuration as that used by Elagin et al., and for an applied voltage of +13.5 kV. In the positive corona, the ionization region is confined to a thin layer around the anode of negligible extent. Therefore, the space charge is essentially positive everywhere, and the electric force is directed towards the cathode along the electric field lines (solid lines). The force magnitude is especially important right below the wire, where both the electric field and the space charge reach their maximum values.

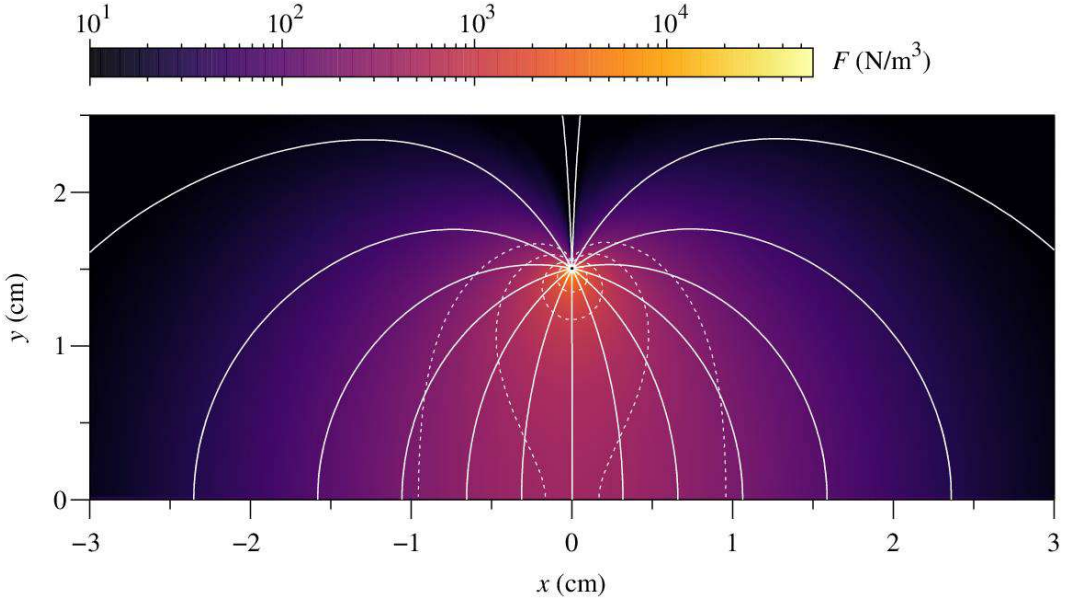

Figure 6. 2D-spatial distribution of the EHD force density magnitude and electric field lines (solid lines) in the vicinity of the wire for an applied voltage V = +13.5 kV (wire radius: r_0 = 50 μm, wire-plate separation: d = 1.5 cm). Isolines of the force density (dashed lines) are drawn at 2×10^3, 10^3, 4×10^2 and 2×10^2 N/m^3.

The 2D gas velocity field generated by this force density, simulated with the RANS k-epsilon turbulence model, is shown in figure 7(a) and can be compared with the experimental measurements by Elagin et al., which are presented in figure 7(b). As can be readily seen, both spatial distributions of velocity are globally very similar. The fluid is accelerated along the symmetry axis and, after impinging on the ground plate, the gas flow is deflected in opposite directions. The regions with the highest fluid velocities are located along the symmetry axis and along the plate. A quantitative comparison can be made based on the maximum values of velocities observed in each case: according to the numerical modeling, the maximum velocity is 3.6 m/s, while according to the experimental observation it is about 3.5 m/s. Therefore, the agreement is quite satisfactory.

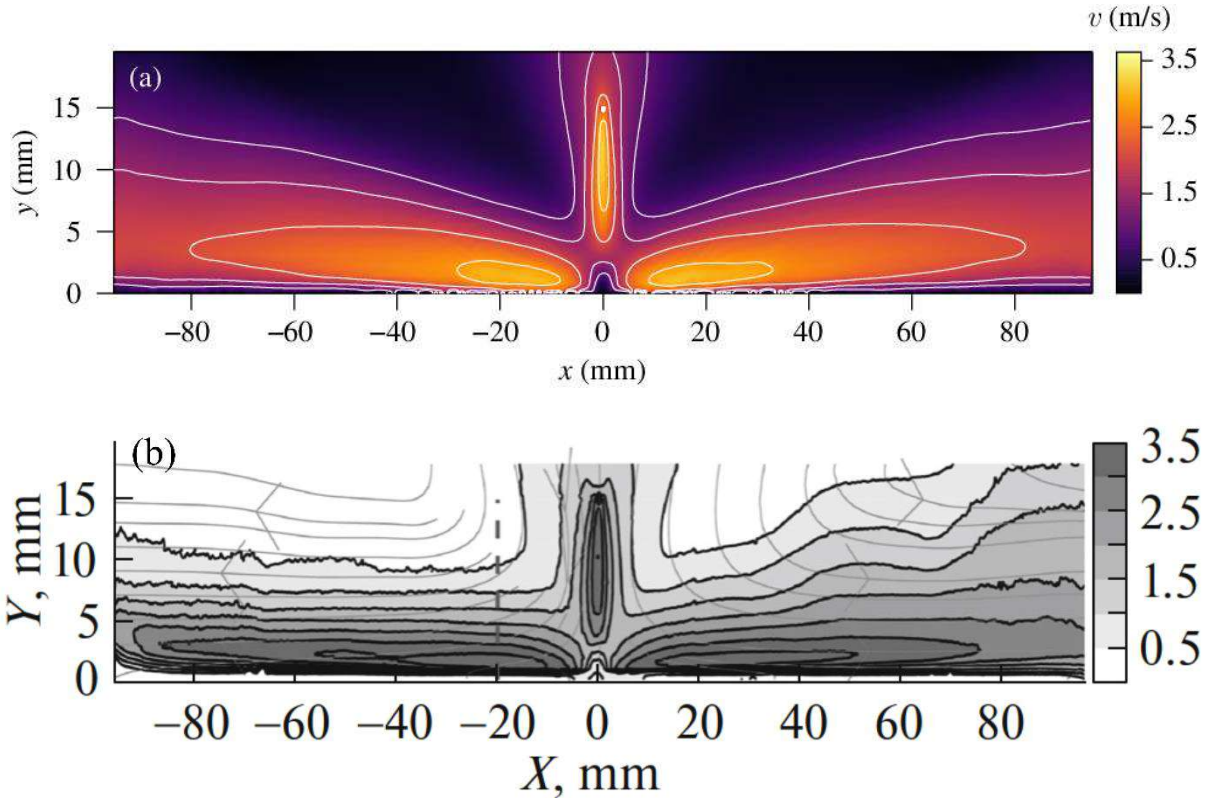

Figure 7. 2D-spatial distribution of the velocity magnitude and their corresponding contour lines for an applied voltage V = +13.5 kV (wire radius: r_0 = 50 μm, wire-plate separation: d = 15 mm). (a) Numerical modeling. Isolines of the velocity magnitude are drawn at 2.8, 2.1, 1.5 and 1 m/s. (b) Experimental measurements using PIV reported by Elagin et al. [38] in Experimental investigation of cooling of a plate by ionic wind from a corona-forming wire electrode, *Technical Physics*, **61** (2016) 1218, Pleiades Publishing, Ltd. Reproduced with permission from SNCSC.

The second electrode arrangement selected for the electrohydrodynamic validation is the one used by Jewell-Larsen et al. [39] in his investigations of EHD air movers based on positive corona discharge. This configuration is of special interest in the development of efficient EHD cooling systems for laptop applications [40]. As shown in figure 8, the geometric configuration corresponds to wire-duct, but the walls of the duct are made of insulating acrylic sheets 7 cm long, spaced 6 mm apart. Two gold-plated aluminum strips stuck to the walls and connected to the ground act as collector electrodes. They used a corona wire of radius r_0 = 12.5 μm and collector strips 5 mm wide, which protruded 0.1 mm from the duct walls. The wire was located 4 cm away from the duct entrance, and the horizontal separation between the center of the wire and the strips was 6 mm.

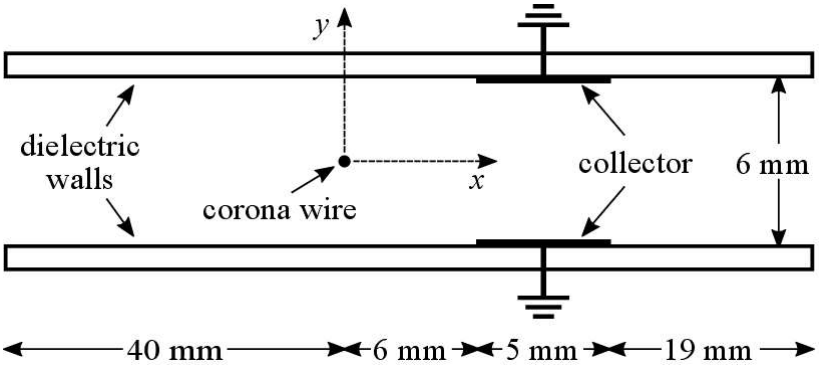

Figure 8. Schematic representation of the EHD air mover device used by Jewell-Larsen et al. [39] (not to scale).

As explained before, the first step to obtain the velocity distribution is to determine the force density from the solution of the electrical equations. An example of such computation is shown in figure 9, where the magnitude of the EHD force density together with the corresponding electric field lines are presented for the same electrode arrangement used by Jewell-Larsen et al., and for an applied voltage of +10 kV on the corona wire. The computational domain shown in this figure has been limited to the region between the anode and the cathode, in which the EHD force is non negligible. As in the wire-plate case, the EHD force is especially important around the corona wire, where it reaches a magnitude of about 1.3×10^5 N/m^3, two orders of magnitude higher than at the grounded electrodes.

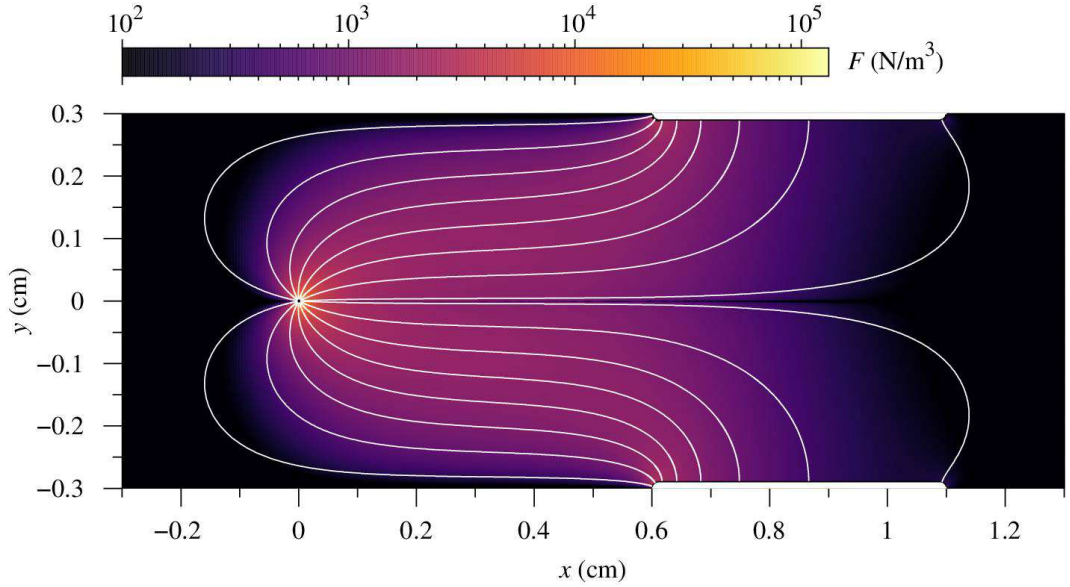

Figure 9. 2D-spatial distribution of the EHD force density magnitude and electric field lines (solid lines) inside the EHD blower, for an applied voltage $V = +10$ kV (wire radius: $r_0 = 12.5$ μm).

Once the EHD force density has been evaluated, the Navier-Stokes equations can be integrated numerically to obtain the spatial distribution of the gas velocity. In addition to the no-slip boundary condition at the solid boundaries, open boundary conditions for the pressure are imposed at the inlet and at the outlet of the duct. The results of the numerical simulation, assuming laminar flow, are presented in figure 10, where both the 2D spatial distribution of the gas velocity magnitude and the corresponding streamlines are plotted. The maximum gas velocity is reached along the axis of symmetry, at the entrance of the collector plates.

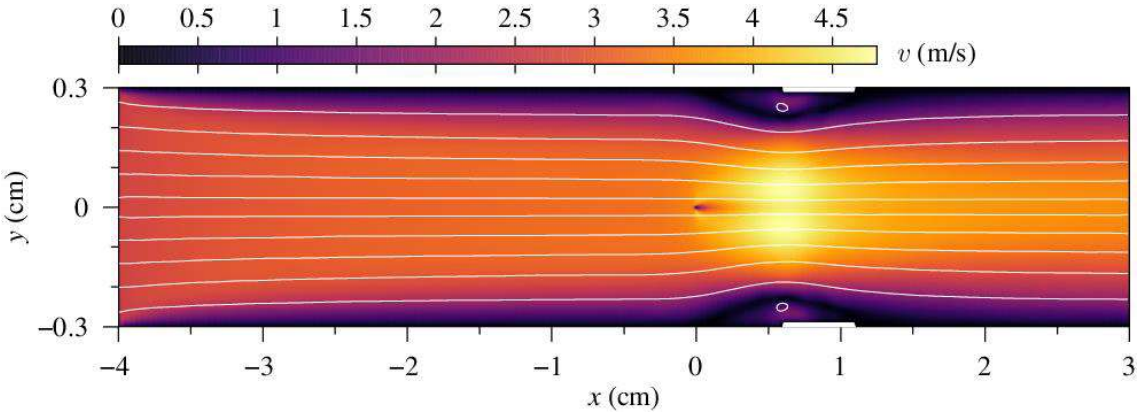

Figure 10. 2D-spatial distribution of the velocity magnitude and their corresponding streamlines for an applied voltage ϕ_0 = +10kV (wire radius: r_0 = 12.5 μm).

To determine the gas flow rate and the averaged velocity at the outlet of the duct, Jewell-Larsen et al. affixed the EHD air mover to a wind-tunnel, where the relative pressure drop across a calibrated nozzle was measured using a digital pressure gauge. In this way, they were able to measure the airflow performance of the device as a function of the input electric power per unit of wire length. Figure 11 shows the measurements of the mean outlet velocity and how they compare with the results of the present numerical simulation. Again, it can be concluded that the numerical modeling accurately reproduces the EHD gas flow generated by the corona discharge in this electrode configuration.

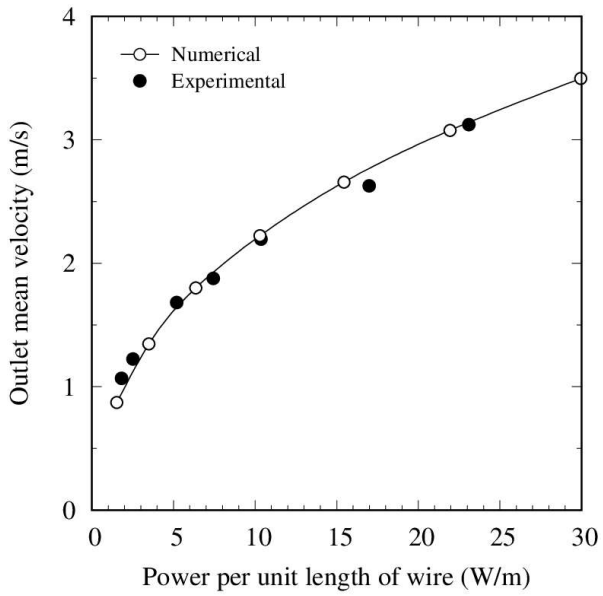

Figure 11. Average velocity at the outlet of the duct as a function of the electric power per unit of length of corona wire according to the numerical simulation and its comparison with experiments. The experimental points (black circles) correspond to the measurements of Jewell-Larsen et al. [39].

3.2 Improved electrode configuration for EHD air movers

As previously explained, the increasing miniaturization of electronic components demands highly efficient cooling solutions to meet heat dissipation requirements. In this context, EHD air pumps present notable advantages over conventional rotary fans, particularly a superior

heat transfer performance for small-scale applications. Ideally, the design of the EHD air pump electrodes should be as simple and robust as possible, without compromising efficiency, which will ensure longer operating time before failure.

The electrode configuration of the EHD air blower shown in figure 8 has the major drawback that the corona wire must be placed equidistant between the two insulating plates. Therefore, as the blower dimensions are reduced, the placement of the corona wire becomes more difficult and error prone. Furthermore, the corona wire intercepts the air flow, and mechanical vibrations of the wire can be induced by the effect of electrical forces [41].

Therefore, in this section, a variation of the electrode configuration considered by Jewell-Larsen et al. [39] is presented. As shown in figure 12, instead of a single corona wire located in the center of the channel, the proposed configuration consists of two corona electrodes of radius r_0 = 12.5 μm half embedded in the dielectric walls that confine the flow. Thus, the effective wire surface for corona discharge is the same as that of a single corona wire. Similarly to [39], two 5 mm wide strips protruding 0.1 mm from the walls act as collectors of the corona discharge current. The wire and the collector strip are also separated by 6 mm.

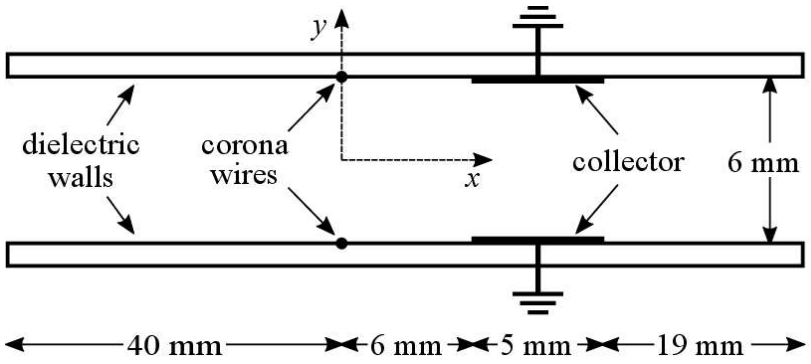

Figure 12. Schematic representation of the improved EHD air mover (not to scale).

Figure 13 shows the numerical simulation results for the current-voltage characteristic corresponding to the new configuration (with two corona wires) and its comparison with the previous one (with one corona wire). The current intensity is somewhat lower in the case of two corona wires, although in both cases it can be fitted satisfactorily assuming a $V(V - V_0)$ dependence, with $V_0 \approx 4.5$ kV. Certainly, in the configuration with two corona wires, the usual shielding effect that arises between adjacent discharge electrodes must be present. However, this effect is counterbalanced by the shorter distance between each corona wire and its nearby collector, which leads to higher values of the ion density, the electric field, and the current density inside the fluid, compared to the case of a single wire. Therefore, the lower current intensity found in the new electrode configuration must be attributed to the way the current density is distributed over the collector strips, which is different in the two cases.

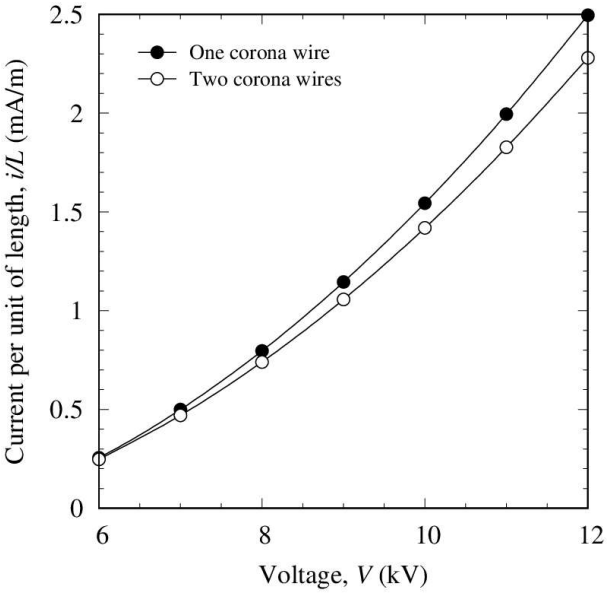

Figure 13. Numerical simulation results for the current-voltage characteristic corresponding to the EHD blower with a single central corona wire (black circles) and two corona wires half embedded in the dielectric walls (white circles).

The 2D-spatial distributions of charge density and electric force density are shown in figures 14 and 15, respectively, for a voltage applied to the wires of 10 kV. The maximum value of the electric force density is about 30 % higher than in the configuration with a single wire, and most of the space charge is distributed in the proximity of the dielectric plates, where the electric field lines run near parallel to them. In contrast, the force density in the central part of the channel is negligible. This situation is completely opposite to that observed in the configuration with a single central wire (figure 9), in which the electric force density was negligible near the dielectric walls, but had an appreciable value near the axis of symmetry.

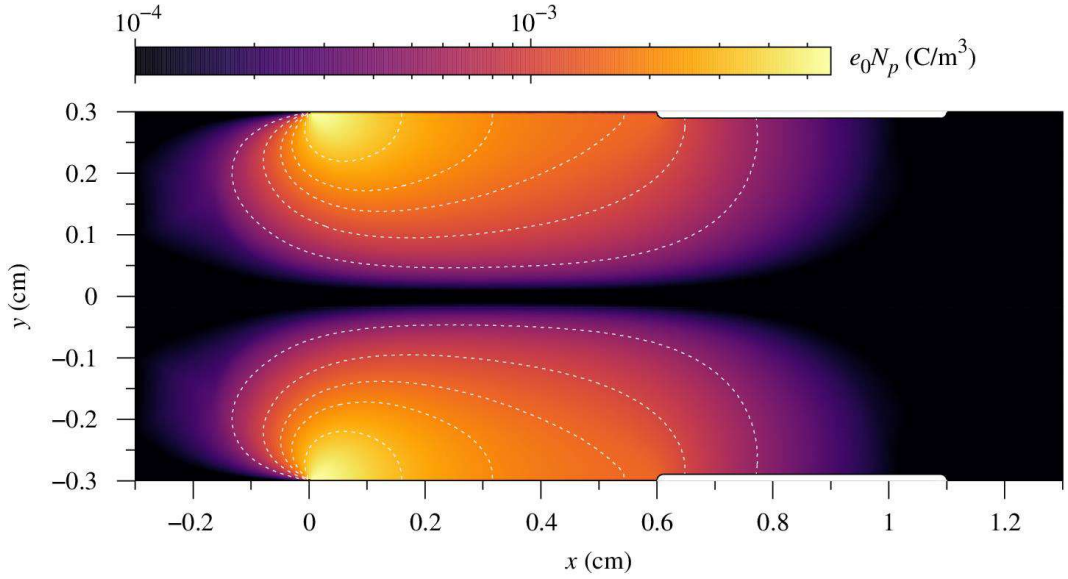

Figure 14. 2D-spatial distribution of the charge density inside the improved EHD blower, for an applied voltage $V = +10$ kV and corona wires of radius $r_0 = 12.5$ μm. Isolines of the charge density (dashed lines) are drawn at 5×10^{-4}, 10^{-3}, 1.5×10^{-3}, 2×10^{-3} and 3×10^{-3} C/m^3.

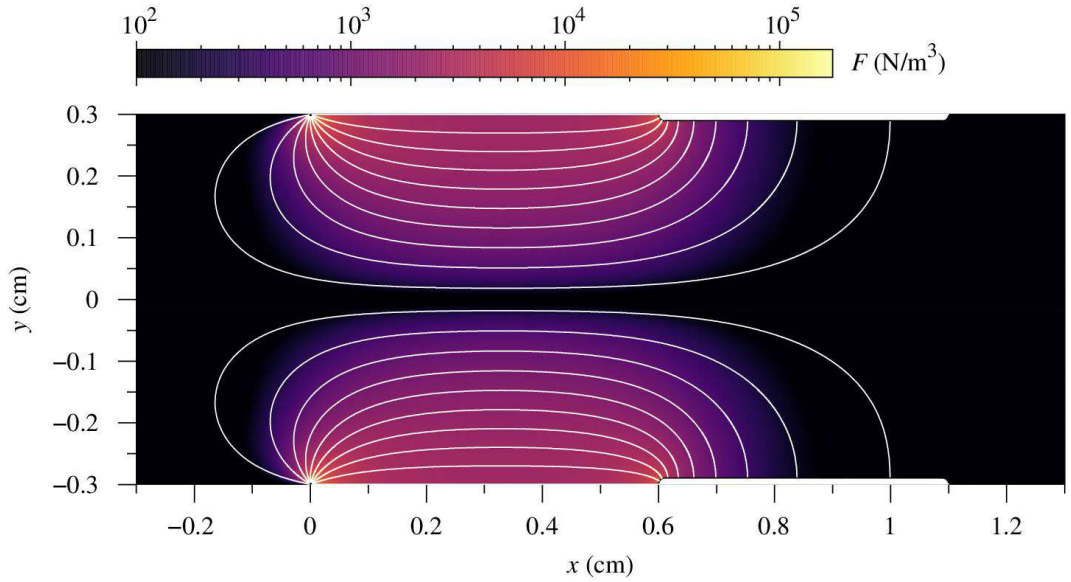

Figure 15. 2D-spatial distribution of the EHD force density magnitude and electric field lines (solid lines) inside the improved EHD blower, for an applied voltage $V = +10$ kV and corona wires of radius $r_0 = 12.5$ μm.

However, the present electrode configuration has the intrinsic advantage of accelerating the fluid next to the walls, where the retarding force due to shear stress is stronger. This fact can clearly be appreciated in figure 16, where the 2D velocity distribution is presented for an applied voltage to the corona wires of 10 kV. It is worth mentioning that the characteristics of this flow pattern are particularly suitable for applications requiring efficient cooling, since a high fluid velocity along the walls enhances heat transfer between the walls and the fluid.

Compared to figure 10, the maximum values of the velocity field are now reached closer to the walls, and further downstream, between the two collector strips. Moreover, the recirculating eddies that previously originated in the vicinity of the collecting strips (see figure 10) have been completely eliminated. Interestingly, although the maximum gas velocity inside the blower in this electrode configuration is about 10 % lower than with a single corona wire, the averaged values of velocity at the exit of the duct are nearly identical (slightly higher in the new configuration). Of course, as shown in figure 17, the velocity profiles are quite different at the outlet, as they still bear the imprint of the upstream EHD force distribution driving the gas flow.

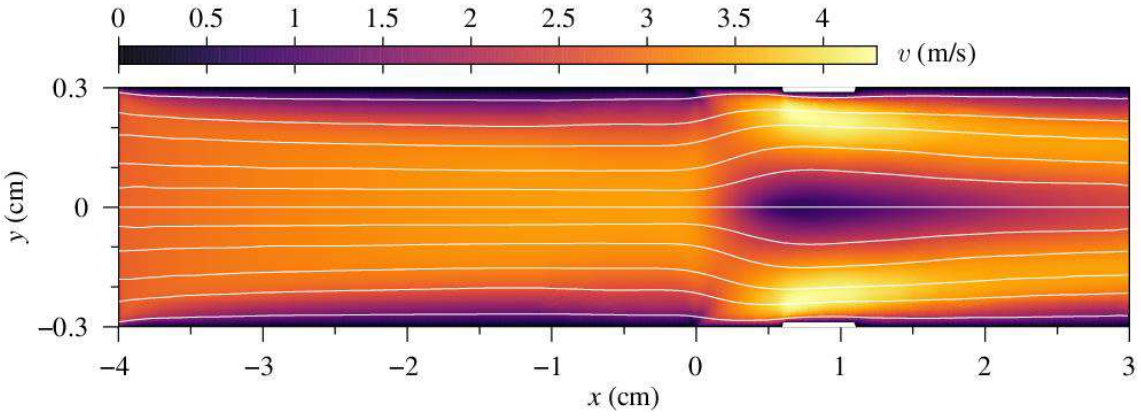

Figure 16. 2D-spatial distribution of the velocity magnitude and their corresponding streamlines inside the improved EHD blower for an applied voltage ϕ_0 = +10kV and corona wires of radius r_0 = 12.5 μm.

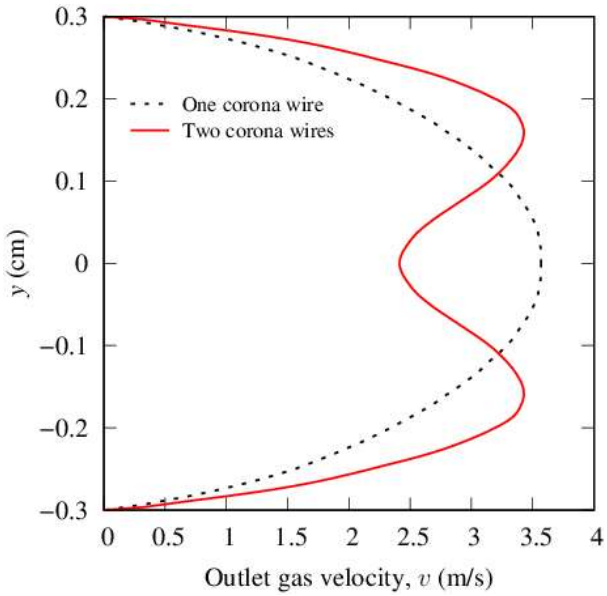

Figure 17. 2D-spatial distribution of the velocity magnitude at the exit of the EHD blower using an electrode configuration with a single central corona wire (dashed line) and two corona wires half embedded in the dielectric walls (solid line). for an applied voltage ϕ_0 = +10kV and corona wires of radius r_0 = 12.5 μm.

Although the electrode arrangement in the improved EHD blower has the aforementioned advantages of simpler construction and superior heat transfer from the walls to the fluid, it would be interesting to determine if these advantages come at the cost of higher energy consumption. To elucidate this question, the averaged outlet velocity is presented as a function of the electrical power in figure 18. In this figure, the numerical simulation results corresponding to the new electrode configuration are directly compared with the experimental measurements carried out by Jewell-Larsen et al. [39], which correspond to a single corona wire. As can be readily seen, for the same electrical power, the outlet velocity is slightly superior when using the modified EHD blower (with two corona wires), especially at the higher electrical powers. Therefore, the proposed electrode arrangement also has better energy efficiency.

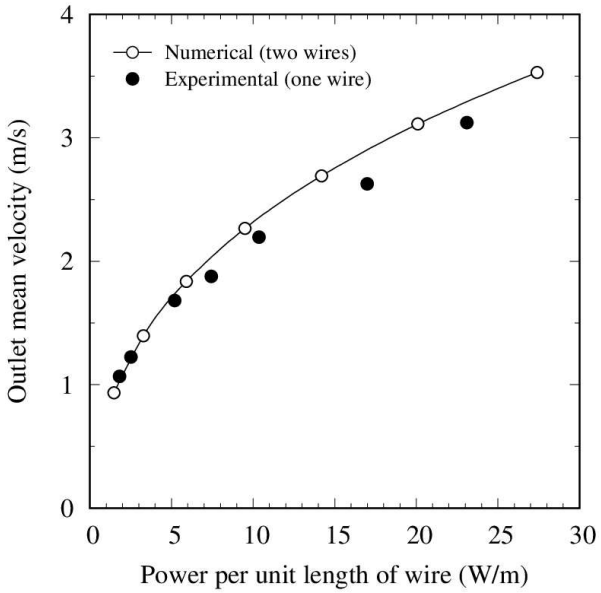

Figure 18. Average velocity at the outlet of the duct as a function of the electric power per unit of length of corona wire according to the numerical simulation and its comparison with experiments. The experimental points (black circles) correspond to the measurements of Jewell-Larsen et al. [39] using a single corona wire.

4 Conclusions

In this paper, we have shown the possibility of successfully modeling a steady corona discharge by taking as the starting point the Laplacian electric field lines and using approximated analytical expressions of the electric field intensity along the field lines. Then, applying a simple root-finding algorithm to match the electric field circulation along each field line to the actual voltage drop, the space charge and the EHD force density can be determined. The proposed approach has the advantage of being able to easily treat arbitrary electrode configurations of practical interest, since only the Laplace equation needs to be integrated numerically. Furthermore, the model is robust, since it avoids the convergence problems that may arise when integrating the Gauss equation coupled to the continuity equation for charge species. And, finally, the solutions provided by the model are computationally unexpensive, which is essential to simulate more complex problems, like the electric wind, which requires a prior knowledge of the EHD force. The accuracy of the solutions provided by the model has been demonstrated by directly confronting its predictions with the experimental measurement of the corona current intensity and the corona current distribution over the cathode.

The suitability of the corona model to obtain the velocity distribution generated by the EHD force has been successfully tested in two different electrode configurations, again comparing with direct experimental observations. Of particular interest is the study of corona wind blowers in narrow channels, as they are being considered for efficient cooling in microelectronics. In this regard, modeling has shown that superior heat transfer performance can be expected by placing the corona wires attached to the duct walls, rather than between the two plates.

Acknowledgement

This work was partially supported by grant PGC2018-099217-B-I00, funded by MCIN/AEI/10.13039/501100011033 and by "FEDER".

References

[1] J.-S. Chang, P. A. Lawless and T. Yamamoto, Corona discharge processes, *IEEE Transactions on Plasma Science* **19** (1991) 1152-1166, doi: 10.1109/27.125038

[2] E. D. Fylladitakis, M. P. Theodoridis, and A. X. Moronis, Review on the History, Research, and Applications of Electrohydrodynamics, *IEEE Transactions on Plasma Science* **42** (2014) 358-375, doi: 10.1109/TPS.2013.2297173

[3] J. Qu, M. Zeng, D. Zhang, D. Yang, X. Wu, Q. Ren, and J. Zhang, A review on recent advances and challenges of ionic wind produced by corona discharges with practical applications, *Journal of Physics D: Applied Physics* **55** (2022) 153002, doi: 10.1088/1361-6463/ac3e2c

[4] B. Komeili, J.S. Chang, G.D. Harvel, C.Y. Ching and D. Brocilo, Flow characteristics of wire-rod type electrohydrodynamic gas pump under negative corona operations, *Journal of Electrostatics* **66** (2008) 342–353, doi: 10.1016/j.elstat.2008.02.004

[5] M. Ghazanchaei, K. Adamiak and G.S.P. Castle, Predicted flow characteristics of a wire-nonparallel plate type electrohydrodynamic gas pump using the Finite Element Method, *Journal of Electrostatics* **73** (2016) 103-111, doi: 10.1016/j.elstat.2014.11.003

[6] J. Wang, T. Zhu, Y.X. Cai, J.F. Zhang, and J.B. Wang, Review on the recent development of corona wind and its application in heat transfer enhancement, *International Journal of Heat and Mass Transfer* **152** (2020), 119545, doi: 10.1016/j.ijheatmasstransfer.2020.119545

[7] N. Zehtabiyan-Rezaie, K. Adamiak, and M. Saffar-Avval, Enhancement of evaporation from liquid surfaces due to electrohydrodynamic flow: A review, *Journal of Electrostatics* **114** (2021) 103630, doi: 10.1016/j.elstat.2021.103630

[8] A. Martynenko, and T. Kudra, Electrically-induced transport phenomena in EHD drying – A review, *Trends in Food Science & Technology* **54** (2016) 63–73, doi: 10.1016/j.tifs.2016.05.019.

[9] M. Belan, L. Arosti, R. Polatti, F. Maggi, S. Fiorini and F. Sottovia, A parametric study of electrodes geometries for atmospheric electrohydrodynamic propulsion, *Journal of Electrostatics* **113** (2021) 103616, doi: 10.1016/j.elstat.2021.103616.

[10] E. Moreau, N. Benard, J.D. Lan-Sun-Luk and J.P. Chabriat, Electrohydrodynamic force produced by a wire-to-cylinder dc corona discharge in air at atmospheric pressure, *Journal of Physics D: Applied Physics* **46** (2013) 475204, doi: 10.1088/0022-3727/46/47/475204

[11] E. Moreau, C. Louste, G. Artana, M. Forte, G. Touchard, Contribution of Plasma Control Technology for Aerodynamic Applications, *Plasma Processes and Polymers* **3** (2006) 697–707, doi: 10.1002/ppap.200600059

[12] C. Guerra-Garcia, N. C. Nguyen, T. Mouratidis, and M. Martinez-Sanchez, Corona discharge in wind for electrically isolated electrodes, *Journal of Geophysical Research: Atmospheres*, **125** (2020) e2020JD032908, doi: 10.1029/2020JD032908

[13] P. Atten, Méthode générale de résolution du problème du champ électrique modifié par une charge d'espace unipolaire injectée, *Revue Général de l'Électricité* **83** (1974) 143–153.

[14] J.R. McDonald, W.B. Smith, H.W. Spencer III and L.E. Sparks, A mathematical model for calculating electrical conditions in wire-duct electrostatic precipitation devices, *Journal of Applied Physics* **48** (1977) 2231–2243, doi: 10.1063/1.324034

[15] J.L. Davies and J.F. Hoburg, Wire-duct precipitator field and charge computation using finite element and characteristics method, *Journal of Electrostatics* **14** (1983) 187–199, doi: 10.1016/0304-3886(83)90006-2

[16] N.A. Kaptsov, *Electric Phenomena in Gases and in Vacuum*, Gostekhizdat, Moscow-Leningrad, 1950.

[17] L. Zhao and K. Adamiak, Effects of EHD and external airflows on electric corona discharge in point-plane/mesh configurations, *IEEE Transactions on Industry Applications* **45** (2009) 16–21, doi: 10.1109/TIA.2008.2009389

[18] L. Zhao and K. Adamiak, Numerical simulation of the effect of EHD flow on corona discharge in compressed air, *IEEE Transactions on Industry Applications* **49** (2013) 298-304, doi: 10.1109/IAS.2011.6074283

[19] P.L. Levin and J.F. Hoburg, Donor cell-finite element description of wire-duct precipitator fields, charges, and efficiencies, *IEEE Transactions on Industry Applications* **26** (1990) 662–670, doi: 10.1109/28.55991

[20] A.J. Medlin, C.A.J. Fletcher and R. Morrow, A pseudo transient approach to steady state solution of electric field-space charge coupled problems, *Journal of Electrostatics* **43** (1998) 39–60, doi: 10.1016/S0304-3886(97)00167-8

[21] B.-L. Qin and P.D. Pedrow, Particle-in-cell simulation of bipolar DC corona, *IEEE Transactions on Dielectrics and Electrical Insulation* **1** (1994) 1104–1118, doi: 10.1109/94.368652

[22] P. Seimandi, G. Dufour and F. Rogier, An asymptotic model for steady wire-to-wire corona discharges, *Mathematical and Computer Modelling* **50** (2009) 574–583, doi: 10.1016/j.mcm.2009.03.005

[23] K. Yanallah, F. Pontiga, Y. Meslem, and A. Castellanos, An analytical approach to wire-to-cylinder corona discharge, *Journal of Electrostatics* **70** (2012) 374-383, doi: 10.1016/j.elstat.2012.05.002

[24] K. Yanallah and F. Pontiga, A semi-analytical stationary model of a point-to-plane corona discharge, *Plasma Sources Science and Technology* **21** (2012) 045007, doi: 10.1088/0963-0252/21/4/045007

[25] K. Yanallah, F. Pontiga and J. H. Chen, A semi-analytical study of positive corona discharge in wire–plane electrode configuration, *Journal of Physics D: Applied Physics* **46** (2013) 345202, doi: 10.1088/0022-3727/46/34/345202

[26] K. Yanallah, F. Pontiga, M. R. Bouazza, and J. H. Chen, The effect of the electric wind on the spatial distribution of chemical species in the positive corona discharge, *Journal of Physics D: Applied Physics* **50** (2017) 335203, doi: 10.1088/1361-6463/aa7b24

[27] M. R. Bouazza, K. Yanallah, F. Pontiga and J. H. Chen, A simplified formulation of wire-plate corona discharge in air: application to the ion wind simulation, *Journal of Electrostatics* **92** (2018) 54-65, doi: 10.1016/j.elstat.2018.02.001

[28] M. Bouadi, K. Yanallah, M.R. Bouazza and F. Pontiga, Effect of the Variation of the Electrode Geometrical Configuration on the Electric Wind Velocity Produced by an Electric Corona Discharge, in A. Belasri, S. Beldjilali, (eds) *ICREEC 2019. Springer Proceedings in Energy*. Springer, Singapore, doi: 10.1007/978-981-15-5444-5_58

[29] S. Ohashi, and K. Hidaka, A method for computing current density and electric field in electrical discharge space using current flow-line coordinate. *Journal of Electrostatics*, **43** (1998) 101-114, doi: 10.1016/S0304-3886(97)00165-4

[30] Y. Guan, R.S. Vaddi, A. Aliseda, and I. Novosselova, Analytical model of electro-hydrodynamic flow in corona discharge, *Physics of Plasmas* **25** (2018) 083507, doi; 10.1063/1.5029403

[31] N.C. Nguyen, C. Guerra-Garcia, J. Peraire, and M. Martinez-Sanchez, Computational study of glow corona discharge in wind: Biased conductor, *Journal of Electrostatics* **89** (2017) 1-12, doi: 10.1016/j.elstat.2017.06.005

[32] K. Adamiak, V. Atrazhev, and P. Atten, Corona discharge in the hyperbolic point-plane configuration: direct ionization criterion versus an approximate formulations. *IEEE Transactions on Dielectrics and Electrical Insulation*, **12** (2005) 1015-1024, doi: 10.1109/TDEI.2005.1522195

[33] M. Goldman, and A. Goldman, (1978) Chapter 4 - Corona Discharges. In Hirsh, M. N. and Oskam, H. J. (Editors), Gaseous Electronics (pp. 219-290). Academic Press, doi: 10.1016/B978-0-12-349701-7.50009-2.

[34] R.S. Sigmond, The unipolar corona space charge flow problem. *Journal of Electrostatics*, **18** (1986) 249-272, doi: 10.1016/0304-3886(86)90021-5

[35] T. Yamamoto, and H. Velkoff, Electrohydrodynamics in an electrostatic precipitator. *Journal of Fluid Mechanics,* **108** (1981) 1-18, doi: 10.1017/S002211208100195X

[36] P. Cooperman, A theory for space-charge-limited currents with application to electrical precipitation, *Transactions of the American Institute of Electrical Engineers, Part I: Communication and Electronics*, **79** (1960) 47-50, doi: 10.1109/TCE.1960.6368541

[37] https://openfoam.org/

[38] I.A. Elagin, V.V. Yakovlev, I.A. Ashikhmin, and Yu. K. Stishkov, Experimental investigation of cooling of a plate by ionic wind from a corona-forming wire electrode. *Technical Physics*, **61** (2016) 1214–1219, doi: 10.1134/S1063784216080077

[39] N.E. Jewell-Larsen, G.G. Joseph, and K.A. Honer, Scaling Laws for Electrohydrodynamic Air Movers. *Proceedings of the ASME/JSME 2011 8th Thermal Engineering Joint Conference*. *ASME/JSME 2011 8th Thermal Engineering Joint Conference*. Honolulu, Hawaii, USA. March 13–17, 2011. T10109. ASME, doi: 10.1115/AJTEC2011-44626

[40] A.A. Ramadhan, N. Kapur, J.L. Summers, H.M. Thompson, Numerical development of EHD cooling systems for laptop applications, *Applied Thermal Engineering*, **139** (2018) 144-156, doi: 10.1016/j.applthermaleng.2018.04.119

[41] M. Kawasaki, and T. Adachi, Mechanism and preventive method of self-excited vibration of corona wire in an electrostatic precipitator, *Journal of Electrostatics* **36** (1996) 235-252, doi: 10.1016/0304-3886(95)00047-X.